

Direct estimation of the distribution of relaxation times from induced-polarization spectra using a Fourier transform analysis

N. Florsch^{1,2}, C. Camerlynck^{1,3} and A. Revil^{4,5*}

¹ Université Pierre et Marie Curie, 75252 Paris, France

² Institut de Recherche pour le Développement IRD-UMI 209 'UMMISCO', 93143 Bondy Cedex, France

³ UMR-CNRS 7619, Sisyphé, Paris, France

⁴ Colorado School of Mines, Department of Geophysics, Golden, 80401, CO, USA

⁵ ISTerre, CNRS, UMR CNRS 5275, Université de Savoie, 73376 Cedex, Le Bourget du Lac, France

Received November 2011, revision accepted February 2012

ABSTRACT

The analysis of low-frequency spectral induced polarization data involves the determination of the distribution of relaxation times either from time-domain or frequency domain measurements. The classical approach is to assume a simple transfer function (e.g., a Cole-Cole function) and to determine, by a deterministic or a stochastic fitting procedure, the parameters of this transfer function (for instance the four Cole-Cole parameters). Some other methods (based on optimization) have been developed recently avoiding the choice of a specific transfer function that can bias data interpretation. We have developed a new approach based on the Fourier transform also avoiding the use of a specific analytical transfer function. The use of the Fourier transform is a classical approach to retrieve the kernel of a Fredholm integral equation of the first kind (especially in potential field theory) and this corresponds exactly to the problem we want to solve. We adapt the Fourier transform approach to retrieve the distribution of the relaxation times (for instance to process low-frequency induced polarization data). Problems resulting from the use of this approach with noisy data are prevented by using Wiener filtering. As far as induced polarization is concerned, we found that it is necessary to fit the high-frequency dielectric contribution of the spectra and to remove this contribution from the quadrature conductivity data before inverting the distribution of the relaxation times. Our approach is benchmarked with analytical pair solutions and then tested by using synthetic and experimental data sets.

INTRODUCTION

Induced polarization is a geophysical method sensitive to the reversible storage of electrical charges in porous media with a number of applications to the localization of ore bodies (Marshall and Madden 1959) and environmental problems including the study of contaminant plumes and bioremediation (Börner *et al.* 1996; Kemna 2000; Binley *et al.* 2005), permeability imaging (Hördt *et al.* 2007) and salt tracer tests (Karaoulis *et al.* 2011). This (non-intrusive) geophysical method can be performed either in the time domain or in the frequency domain. In the frequency domain, it consists in measuring the resistivity and phase lag between the alternating current and the voltage response in a broad frequency range (typically from 1 mHz and 1 kHz or more recently 12 or 20 kHz thanks to fibre optic-based systems). The interpretation of induced polarization measurements involves the

determination and interpretation of the distribution of the relaxation times either from time-domain data (Tong *et al.* 2006a,b; Tarasov and Titov 2007) or from frequency domain data (Kemna 2000; Ghorbani *et al.* 2007; Chen *et al.* 2008). The literature devoted to the determination of the distribution of relaxation times can be divided into two classes of methods depending on whether specific analytical transfer functions are used or not.

In the first class of methods, the distribution of relaxation times is supposed to be analytically known and its mathematical formula is explicitly given. Examples include the Debye distribution, the Cole-Cole distribution and the Cole-Davidson distribution among many other functions. Then the problem lies in the determination of the parameters involved in the analytical model using either deterministic or stochastic approaches (Kemna 2000; Ghorbani *et al.* 2007; Chen *et al.* 2008 and references therein). In this case, the inverse problem consists in fitting the data to invert a few model parameters (e.g., three if the Debye

*arevil@mines.edu

function is adopted and four for the Cole-Cole function). The most used analytical model to interpret spectral induced polarization data remains the Cole-Cole model (Cole and Cole 1941; see Ghorbani *et al.* 2007 for a Bayesian analysis of this function both in time and frequency domains). A number of authors have also used models based on modifications of the Cole-Cole model like the double Cole-Cole model (Chen *et al.* 2008; Ghorbani *et al.* 2009) and the generalized Cole-Cole model (Davidson and Cole 1950; Vanhala 1997; Pelton *et al.* 1983; Ghorbani *et al.* 2009). There are many other models that have been proposed in the literature. For instance, Dias (2000) discussed 12 analytical functions in the frequency domain while Yeung and Shin (1991) proposed 13 analytical functions in the time domain. The paper by Macdonald and Brachman (1956) mentioned 21 analytical functions. These authors provided both the transfer functions and the time functions and their associated (normalized) distributions of relaxation times $g_r(\tau)$. However, most of these models are not suitable to interpret the geophysical response of earth materials (curiously the Cole-Cole model is not cited by Macdonald and Brachman 1956). Such a high number of models is not satisfying even if some attempts have been made to propose more general models (e.g., Yeung and Shin 1991).

In our opinion, this abundance of analytical models results from the high number of ways the relaxation times can be distributed (scattered) over the investigated range of frequencies. It is also a consequence of trying to handle the mathematical representation of the IP spectra as canonical as possible. For instance, the Cole-Cole model combines a rather simple distribution density (see equation (13) in Cole and Cole 1941) with a 'simple' generalization of Debye's model using an exponent in its frequency dependant term. Such a generalization is also broadly used to characterize the rheology of viscoelastic porous materials for the same reasons (see for instance Revil *et al.* 2006). As pointed out by Cole and Cole themselves, the so-called Cole-Cole probability distribution for the relaxation times is not really different from a log-normal distribution (see equation (12) and Fig. 9 in Cole and Cole 1941). However, to the best of our knowledge, the transfer function that would correspond to the log-normal law for the distribution of relaxation times has never been described in the literature and, despite the efforts of many researchers (and ours too), remains analytically unreachable.

In the second class of methods, the distribution of relaxation times may be obtained without specifying any prior analytical functions. The method described in the present paper belongs to this second class of methods. We want to find the distribution of relaxation times using a discrete spectrum analysis. Recovering the distribution of relaxation times by using the inverse problem theory has already been described by several authors (Tong *et al.* 2006a,b; Tarasov and Titov 2007; Nordsiek and Weller 2008; Zisser *et al.* 2010). In the time domain, the method proposed by Tarasov and Titov (2007) is based on Tikhonov regularized optimization. Although the time-domain induced polarization is much less

efficient to retrieve induced polarization parameters than the frequency domain polarization (SIP) method (see Ghorbani *et al.* 2007 for a discussion), Tarasov and Titov (2007) obtained impressive and meaningful results for saturated sands. Tong *et al.* (2006a,b) also obtained very good results in inverting time-domain IP data using the Singular Value Decomposition (SVD) method and used their results to infer the permeability of sandstones.

In the present paper, we develop a new and simple approach based on the Fourier transform. It requires no prior information regarding the structure of the distribution of relaxation times. Despite the fact that the method developed below has been suggested very early in the induced polarization literature (for instance by Fuoss and Kirkwood 1941), to the best of our knowledge, it has never been actually developed and used.

FORMULATION OF THE PROBLEM

We consider below the case of frequency domain IP data. When considering a box-representation of a linear system (in the frequency domain) with an input signal $X(\omega)$ and an output signal $Y(\omega)$, the transfer function of the system (corresponding to the complex-valued impedance in our case) can be written, with an additional additive constant for more generality, as:

$$Y(\omega) = Z_\omega(\omega) X(\omega) \quad (1)$$

$$Z_\omega(\omega) = \frac{a}{1+i\omega\tau} + b, \quad (2)$$

where ω is the angular frequency, τ a (real) relaxation time (in s) and a and b are two real (or possibly complex) constants. If Z corresponds to the impedance, then a and b are expressed in Ohm (Ω). As far as electromagnetic signals are concerned, this model is usually named the Debye's model in honour of the physicist Peter J.W. Debye (Debye and Falkenhagen 1928; Strauss 1954). Equation (2) is also used to treat some rheological problems (it is called the Maxwell model in fluid dynamics in the case of simple viscoelastic media) or any (linear) phenomenon where a basic relaxation occurs described by a single relaxation time. The Debye model also plays an important role in the study of dielectrics (Jonscher 1983, 1999). In this case, the effective dielectric constant ε^* is written as:

$$\varepsilon^* = \varepsilon_\infty + \frac{\varepsilon_0 - \varepsilon_\infty}{1+i\omega\tau}, \quad (3)$$

or alternatively

$$\frac{\varepsilon^* - \varepsilon_\infty}{\varepsilon_0 - \varepsilon_\infty} = \frac{1}{1+i\omega\tau} \quad (4)$$

where $i^2 = -1$ (i represents the pure imaginary number) and ε_0 and ε_∞ represent the asymptotic dielectric constants at zero and infinite frequency, respectively. In geophysics, the Debye model has been used to fit the (low-frequency) Induced Polarization (IP) response of porous rocks for which the polarization effect is usu-

ally non-dielectric in nature (Lesmes and Morgan 2001; Leroy *et al.* 2008; Revil and Florsch 2010; Vaudelet *et al.* 2011). For the Debye model, the complex resistivity can be written as,

$$\rho^*(\omega) = \rho_0 \left[1 - m \left[1 - \left(\frac{1}{1 + i\omega\tau} \right) \right] \right] \quad (5)$$

where $m = (\rho_0 - \rho_\infty)/\rho_0$ (dimensionless, $0 \leq m \leq 1$) denotes the chargeability of the material and ρ_0 and ρ_∞ represent the DC resistivity ($\omega = 0$) and the resistivity at infinite frequency, respectively. Usually the high-frequency resistivity can be difficult to evaluate, as discussed later, because of the superposition of the dielectric effect to the low-frequency (non-dielectric) IP effects (see Appendix A and B). Equation (5) corresponds to the same type of expression as equations (3) and (4).

In a linear porous material, the superposition principle applies. Under the assumption that spectral induced polarization can be explained by a linear model and a combination of linear contributions, the superposition of scattered time constants with a (normalized) density function $g_\tau(\tau)$ implies the following generalization:

$$Z_\omega(\omega) = b + a \int_0^\infty \frac{g_\tau(\tau)}{1 + i\omega\tau} d\tau \quad (6)$$

The constant a could be included in $g_\tau(\tau)$ but if $g_\tau(\tau)$ is assimilated to a probability density function (the sum of the probabilities is equal to 1), then we keep the amplitude term a outside the integral and assume that,

$$\int_0^\infty g_\tau(\tau) d\tau = 1. \quad (7)$$

An example of an induced polarization model satisfying equation (6) is discussed in Appendix A. A discussion of the applicability of the superposition principle in spectral induced polarization is also needed and very often such a discussion is missing in papers developing methods to reconstruct the distribution of relaxation times. In the theory developed recently by Revil and Florsch (2010), the superposition principle holds and the local governing equations are linear. More generally, available theories are based on linearization of the governing equations (see Fixman 1980; Dukhin and Shilov 2002 for some examples of first-order linearization of the governing equations in IP). Generally speaking, the IP problem can be non-linear (Olhoeft 1985). Membrane polarization is an example of a non-linear IP contribution showing a non-linear relationship between the current and the voltage because of the existence of a threshold current (Urtenov *et al.* 2007). Olhoeft (1985) showed from laboratory data that some IP data are non-linear and characterized by harmonic distortions, especially at very low frequencies (below 100 mHz). If the contribution to induced polarization is non-linear (showing harmonic distortions), then the superposition principle does not hold and the present approach is not valid.

We now come back to the distribution of relaxation times and its physical meaning. In the theory developed recently by Revil

and Florsch (2010), the distribution of the time constants follows the distribution of the grain sizes themselves due to the relationship between these two parameters expressed as (Schwarz 1962; Revil and Florsch 2010):

$$\tau = \frac{d^2}{2D}, \quad (8)$$

where d is the grain diameter (in m) and D the coefficient of diffusion of the counterions in the Stern layer in the case of the relaxation of the inner part of the electrical double layer. It may be possible however that the distribution of the relaxation times is related to the pore size distribution as suggested by various authors (Scott and Barker 2003; Kruschwitz *et al.* 2010). In their study of the induced polarization response of pyrite, Pelton *et al.* (1978) showed, using the experimental data of Grisseman (1971), that the time constant from IP data depends also on the square of the grain diameter of the pyrite grains (see his Fig. 6 for which two decades in the distribution of the time constants fit linearly one decade in the mean grain size of the pyrite grains). In sedimentary rocks, the grain size and pore size distributions are often observed to follow a log-normal law or sometimes fractal behaviour over several scales. In both cases, the distribution of the time constants would follow a similar behaviour.

Considering that in real rock, the grain size probability density function is rarely distributed as a narrow peak but follows a broad distribution, the distribution of the relaxation times is expected to be broad (see discussion in Vinegar and Waxman 1984; Lesmes and Morgan 2001; Revil and Florsch 2010). Even in the case where the interaction between the grains is taken into account (Cosenza *et al.* 2008; Zhdanov 2008; Tabbagh *et al.* 2009), the superposition principle applies and can be used to establish the macroscopic response. In the present paper, we consider that the principle of superposition applies.

The time response (or 'impulse response') $g_\tau(\tau)$ associated with equation (3) is given by its inverse Laplace transform,

$$\varphi(t) = b\delta(t) + a \int_0^\infty \frac{g_\tau(\tau)e^{-t/\tau}}{\tau} d\tau \quad (9)$$

This time function may be convoluted with the current to predict the (voltage) response of the medium in the time domain. For more details on time functions, the readers are directed to Yeung and Shin (1991).

We do not try in the next sections to account directly for the high-frequency dielectric term, which is analysed specifically in Appendix B. We consider therefore a set of measurements represented by the model:

$$Z_k = b + a \int_0^\infty \frac{g_\tau(\tau)}{1 + i\omega_k\tau} d\tau + \text{residues}_k, \quad (10)$$

with $k = 1, \dots, K$, where K is the number of involved frequencies. The goal of the present paper is to propose a general method to retrieve $g_\tau(\tau)$ from these data sampled in the frequency domain.

USE OF THE FOURIER TRANSFORM THEORY

From a mathematical standpoint, equations (9) and (10) are called Fredholm integral equations of the first kind. If it is known that for such type of equations, in the case of a convolutive kernel, the kernel itself can be retrieved by using a Fourier transform approach (see for instance Polyanin and Manzhirov 1998). The transformation of equation (4) or equation (7) into a convolutive form is a classic approach in geophysics to solve potential field problems. We consider the arbitrary relaxation time τ_0 and we use the following substitutions:

$$z = -\ln(\omega\tau_0) \Leftrightarrow \omega\tau_0 = e^{-z}, \quad (10)$$

$$s = \ln\left(\frac{\tau}{\tau_0}\right) \Leftrightarrow \tau = \tau_0 e^s, \quad (11)$$

$$G_s(s) = \tau g_\tau(\tau). \quad (12)$$

So z is exchanged with the angular frequency ω and the variable s replaces the relaxation time τ . We have to deal now with the following convolution,

$$Z_z(z) = b + a \int_{-\infty}^{\infty} \frac{G_s(s)}{1 + ie^{-(z-s)}} ds. \quad (13)$$

Finding the distribution $G_s(s)$ replaces the search for the function $g_\tau(\tau)$. Most of the literature emphasizes that making use of the imaginary (quadrature) component of the impedance only is sufficient to retrieve the time distribution and that the additional use of the real part is not useful because it is much less sensitive to the distribution of the relaxation times (see for instance Barsoukov and Macdonald 2005, p. 199). This principle could be derived from signal-to-noise ratio considerations. Indeed, the real part of the impedance (resistivity) involves the dominant constant b (e.g., given by the conductivity of the pore water divided by the formation factor in Appendix A in absence of surface conductivity) while the imaginary part does not involve any additive constant. In the model of Revil and Florsch (2010), the imaginary part of the conductivity is directly proportional to the frequency dependent surface conductivity. The constant b is generally much greater than the variation of the real part itself (see a recent example in Vaudelet *et al.* 2011). Therefore, the presence of a relative random noise (e.g., taken constant over the whole spectrum) would correspond to a higher absolute error on the real part of the impedance. However, the previous reasoning may fail when considering homogeneous absolute errors in the data. Miranda and Rivera (2008) showed for instance how the real part can only be used to invert the Cole-Cole parameters. However, their approach has never been followed by geophysicists. Miranda and Rivera (2008) used the Kramers-Kronig relationships, which connect the real and imaginary parts of a linear causal system. Although we only discuss the imaginary part in this paper, our approach can therefore be adapted to the real part of the complex impedance as well.

Taking the imaginary part of equation (13) and including the constant a into the integral yields:

$$Z_z''(z) = -a \int_{-\infty}^{\infty} G_s(s) \frac{1}{2 \cosh(z-s)} ds = - \int_{-\infty}^{\infty} H_s(s) \frac{1}{2 \cosh(z-s)} ds. \quad (14)$$

The distribution $H_s(s) = aG_s(s)$ is just the same as $G_s(s)$ but not yet normalized. We should remember that $G_s(s)$ is a (normalized) probability density distribution function with the property:

$$\int_{-\infty}^{\infty} G_s(s) ds = 1. \quad (15)$$

Note that constant a can only be determined at the end of the inversion process, once $H_s(s)$ has first been obtained. Therefore we will use $H_s(s)$ in the following analysis. Taking the Fourier Transform (FT) of equation (14) yields,

$$FT[Z_z''] = -\frac{1}{2} FT[H_s] \cdot FT\left[\frac{1}{\cosh}\right]. \quad (16)$$

We use below the symbol ' \sim ' to denote the Fourier Transform (FT). We use the frequency η in this Fourier space (this frequency has nothing to do with the angular frequency ω), we then have the explicit relationship:

$$\tilde{Z}_\eta''(\eta) = -\frac{1}{2} \tilde{H}_\eta(\eta) \cdot FT_\eta\left[\frac{1}{\cosh}\right]. \quad (17)$$

The Fourier transform of the hyperbolic secant function is given by:

$$FT_\eta\left[\frac{1}{\cosh}\right] = \frac{\pi}{\cosh(\pi^2 \eta)}. \quad (18)$$

From equations (17) and (18), we obtain,

$$\tilde{Z}_\eta''(\eta) = -\frac{\pi}{2} \tilde{H}_\eta(\eta) \cdot \frac{1}{\cosh(\pi^2 \eta)}. \quad (19)$$

Using a back Fourier transform, this yields the following expression for $H_s(s)$:

$$H_s(s) = FT^{-1}\left[\tilde{H}_\eta(\eta)\right] = -\frac{2}{\pi} FT^{-1}\left[\tilde{Z}_\eta''(\eta) \cosh(\pi^2 \eta)\right], \quad (20)$$

The inversion of the time distribution is known to be an ill-posed problem in Tikhonov's sense and this is why regularization techniques are required to solve the least-square inversion scheme (Tarasov and Titov 2007). This difficulty appears clearly when considering the equations derived above. Indeed, the spectrum of the data may contain some noise and hence the multiplication by the hyperbolic cosine function normally devoted to recover the initial information blows up the high-frequency content of the noisy data. The so-called Wiener deconvolution, an adaptation of the Wiener filtering approach (Wiener 1949), is a standard signal processing approach to avoid such an artefact in the frequency domain. It is equivalent to a damped least square solution (see Proakis and Manolakis 2007 for a demonstration).

Instead of the equations above, the Wiener deconvolution (see a complete analysis in Appendix C) takes the form that replaces $[\tilde{H}_\eta(\eta)]$ by,

$$\tilde{H}_\eta^w(\eta) = -\frac{2 \tilde{Z}_\eta''(\eta) \cosh(\pi^2 \eta)}{\pi 1 + \cosh^2(\pi^2 \eta) W}, \quad (21)$$

(taking into account the fact that the function ‘cosh’ is purely real) where $W = \text{var}(\tilde{N}(\eta)) [\text{var}(\tilde{Z}_\eta''(\eta))]^{-1}$ and $\text{var}(\tilde{Z}_\eta''(\eta))$ and $\text{var}(\tilde{N}(\eta))$ are the variances (or energy) of the ‘input’ and noise, respectively, both as a function of the frequency. The result is optimal in the Wiener sense and is finally given by:

$$H_s^w(s) = FT^{-1} [\tilde{H}_\eta^w(\eta)] = FT^{-1} \left[-\frac{2 \tilde{Z}_\eta''(\eta) \cosh(\pi^2 \eta)}{\pi 1 + \cosh^2(\pi^2 \eta) W} \right]. \quad (22)$$

Some details on Wiener optimum deconvolution as applied here are discussed in Appendix C. Equation (22) is the main equation derived in our paper. Once the distribution $H_s(s)$ is obtained, it

can be normalized, which yields the function $G_s(s)$ and the constant a and then it is straightforward to retrieve the distribution of the relaxation times using equation (12).

It is frequent that $\text{var}(\tilde{Z}_\eta''(\eta))$ and $\text{var}(\tilde{N}(\eta))$ are difficult to estimate. In such a situation, an optimum W can be estimated by a procedure similar to the one used to estimate the damping parameter while performing a Tikhonov-like regularization of an inverse problem. A popular technique is the so-called L-curve approach. Agarwal (2003) provided an explicit definition of this approach: the ‘‘L-curve is a log-log plot between the squared norm of the regularized solution and the squared norm of the regularized residual for a range of values of regularization parameters’’ (see also Hansen and O’Leary 1993). The advantage of this procedure is its simplicity but it drops a possible dependence of the variances with respect to η . Appendix C contains additional information about the L-curve approach and its use.

Model	$g_s(\tau)$	$Z_\omega(\omega) = \int_0^\infty \frac{g_s(\tau)}{1+i\omega\tau} d\tau$
1	Debye $g(\tau) = \delta(\tau - \tau_0)$	$\frac{1}{1+i\omega\tau_0}$; $\text{Re} = \frac{1}{1+\omega^2\tau_0^2}$; $\text{Imag} = \frac{-\omega\tau_0}{1+\omega^2\tau_0^2}$
2	Cole-Cole (2) $g(\tau) = \frac{1}{2\pi\tau} \frac{\sin \alpha\pi}{\cosh\left[(1-\alpha)\log\left(\frac{\tau}{\tau_0}\right)\right] - \cos \alpha\pi}$	$\frac{1}{1+(i\omega\tau_0)^{1-\alpha}}$; $\text{Re} = \frac{1}{2} \left[1 - \frac{\sinh(1-\alpha)\log(\omega\tau_0)}{\cosh[(1-\alpha)\log(\omega\tau_0)] - \cos \alpha\pi} \right]$; $\text{Imag} = \frac{1}{2} \frac{\cos(\alpha\pi/2)}{\cosh[(1-\alpha)\log(\omega\tau_0)] + \sin(\alpha\pi/2)}$
3	Davidson-Cole (3) $g(\tau) = \frac{\sin \beta\pi}{\pi} \left(\frac{\tau}{\tau_0 - \tau}\right)^\beta$ if $\tau < \tau_0$ $g(\tau) = 0$ if $\tau \geq \tau_0$	$\frac{1}{(1+i\omega\tau_0)^\beta}$; with $y = a \tan(\omega\tau_0)$ $\text{Re} = \cos \beta y (\cos y)^\beta$; $\text{Imag} = -\sin \beta y (\cos y)^\beta$
4	« CPE » Constant Phase Element $g(\tau) = \frac{\sin \beta\pi}{\pi} \tau^{-\beta}$ Only valid if $0 < \beta \neq 1$.	$-\omega^{\beta-1} e^{i\frac{\pi}{2}(\beta-1)}$ $\text{Imag} = -\omega^{\beta-1} \sin\left(\frac{\pi}{2}(\beta+1)\right)$
5	$g(\tau) = 1/\tau, \tau \in I_{\tau_1, \tau_2}$ (4) $g(\tau) = 0, \tau \notin I_{\tau_1, \tau_2}$	$\text{Re} = \ln\left(\frac{\tau_2}{\tau_1} \sqrt{\frac{1+\omega^2\tau_1^2}{1+\omega^2\tau_2^2}}\right)$. (1) $\text{Imag} = \tan^{-1}(\omega\tau_1) - \tan^{-1}(\omega\tau_2)$
6	Williams & Watt (1970) (5) $\frac{1}{2\sqrt{\pi\tau_0}} \exp\left(-\frac{\tau}{4\tau_0}\right)$	$\frac{\sqrt{\pi}}{2\sqrt{\tau_0}} \exp\left(\frac{1}{\tau_0}\right) \text{erfc} \frac{1}{\sqrt{i\omega\tau_0}}$
7	Kirkwood and Fuoss (1941) (6) $\frac{2}{\pi} \frac{\cos\left(\frac{\alpha\pi}{2}\right) \cosh\left(\alpha \log\left(\frac{\tau}{\tau_0}\right)\right)}{\cos^2\left(\frac{\alpha\pi}{2}\right) + \sinh^2\left(\alpha \log\left(\frac{\tau}{\tau_0}\right)\right)}$	$\text{Imag} = \frac{1}{\cosh\left(\alpha \log\left(\frac{\tau}{\tau_0}\right)\right)}$

TABLE 1

Time and frequency domain expressions of some classical transfer functions.

- (1) Our solution. The solution of Matsumoto and Higasi (1962) seems to have a typo.
- (2) From Barsoukov and MacDonald (2005, p. 37). Their equation (40) has a typo.
- (3) From Barsoukov and MacDonald (2005, p. 40).
- (4) $I_{\tau_1, \tau_2} = [\tau_1, \tau_2]$. We shall also use I_{τ_1, τ_2} for the corresponding index function. From Barsoukov and MacDonald (2005, p. 38, 39). Note that this function is not normalizable if it is not restricted to an upper and a lower limit of τ .
- (5) From Williams and Watt (1970) with their $\alpha=1/2$.
- (6) From Barsoukov and Macdonald (2005). Actually the correspondence between their equations (48) and (52) seems to have an error.

TESTS USING SOME ANALYTICAL FUNCTIONS

Some pairs of analytical transfer functions and their associated time constant distributions are used to test the proposed method. They are given in Table 1. Note that the frequency response relative to the very important log-normal distribution remains unsolved analytically despite the effort of various researchers (John Stockwell, personal communication, 2011). However, using the change of variables into the log of the log-normal distribution, the numerical integration of log-normal distribution is possible.

The case of the Debye model: a tautological check

We first test our approach to the most straightforward case corresponding to the Debye distribution. This is to test the self-consistency of our approach in this elementary case. In the Debye case, the distribution of the relaxation times (with $\tau_0 > 0$) is given by,

$$g_\tau(\tau) = \delta(\tau - \tau_0), \tag{23}$$

from which we obtain,

$$G_s(s) = \tau \delta(\tau_0 e^s - \tau_0) = \tau_0 \delta(\tau_0(e^s - 1)) = \frac{\tau_0}{\tau_0} \delta(e^s - 1) = \delta(e^s - 1) = \delta(s). \tag{24}$$

Then, the imaginary part of the transfer function becomes:

$$Z_z''(z) = -\frac{1}{2} \int_{-\infty}^{+\infty} \frac{\delta(s)}{\cosh(z-s)} ds = -\frac{1}{2 \cosh z}. \tag{25}$$

The Fourier transform of this quantity is $1/\cosh$, hence:

$$\tilde{Z}_\eta''(\eta) = -\frac{\pi}{2 \cosh(\pi^2 \eta)}. \tag{26}$$

We apply equation (20) in order to determine $G_s(s)$. This yields

$$\begin{aligned} G_s(s) &= -\frac{2}{\pi} FT^{-1} \left[\tilde{Z}_\eta''(\eta) \cosh(\pi^2 \eta) \right] \\ &= -\frac{2}{\pi} FT^{-1} \left[-\frac{\alpha\pi}{2 \cosh(\pi^2 \eta)} \cosh(\pi^2 \eta) \right], \\ &= FT^{-1} [1] \\ &= \delta(s) \end{aligned} \tag{27}$$

as expected.

Test on a synthetic example

For this synthetic example, we use a weighted combination of Cole-Cole (weight = 1) and $1/\tau$ (weight = 0.2) distributions (cases 2 and 5 from Table 1). The related transfer function (imaginary part only) is therefore given by:

$$Z_\omega''(\omega) = \left\{ \frac{1}{2} \frac{\cos(\alpha\pi/2)}{\cosh[(1-\alpha)\log(\omega\tau_0)] + \sin(\alpha\pi/2)} \right\} + 0.2 \left\{ \tan^{-1}(\omega\tau_1) - \tan^{-1}(\omega\tau_2) \right\}. \tag{28}$$

We use here the following values $\alpha=0.3$, $\tau_0=0.1$, $\tau_1=0.1$, and $\tau_2=10$. The respective distribution of time constants (DTC) is known to be (Fuoss and Kirkwood 1941; Cole and Cole 1941, see Table 1):

$$\gamma_\tau(\tau) = \left\{ \frac{1}{2\pi\tau} \frac{\sin(\alpha\pi)}{\cosh[(1-\alpha)\log(\tau/\tau_0)] - \cos(\alpha\pi)} \right\} + 0.2 \left\{ \frac{1}{\tau} I_{\tau_1, \tau_2} \right\}. \tag{29}$$

We use the notation $\gamma_\tau(\tau)$ instead of $g_\tau(\tau)$ because this function is not normalized. We compute numerically the transfer function on a set of realistic frequency values $\{\omega_k, k=1, \dots, K\}$, where K is the total number of discrete frequencies. We therefore obtained a synthetic data set to which we added a synthetic noise v_k simulating some experimental uncertainties. We take here Gaussian noise with a standard deviation on the quadrature contribution of $5 \cdot 10^{-4}$. Therefore, we consider the contaminated synthetic ‘simulated’ data:

$$Z_{z,k}''^{simulated} = Z_z''(\omega_k) + v_k, \tag{30}$$

where v_k corresponds to the noise. One difficulty lies on the choice of the frequency interval to be used to perform the calculation in the spectral domain. For this example, we choose first a

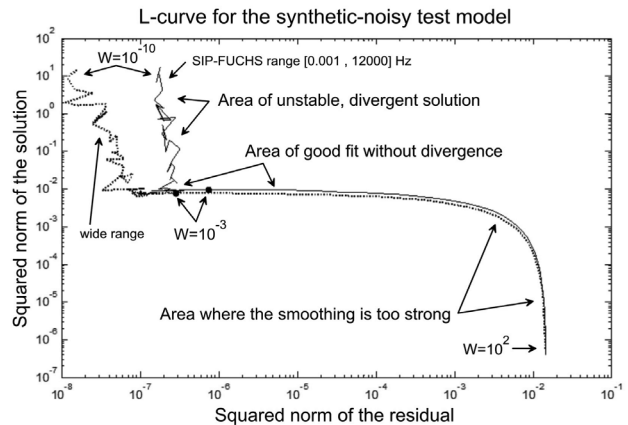


FIGURE 1 L-curves relative to the combined noisy synthetic model, which involves the sum of a Cole-Cole curve with parameters ($\tau_0=0.1; \alpha=0.3 \Leftrightarrow c=0.7$) and a $1/\tau$ model within the interval $\tau \in [0.1; 10]$ s. Two L-curves are shown, related to two frequency ranges, a wide one, which is within $[10^{-8}, 10^8]$ Hz (dotted line) and a ‘SIP-FUCHS’ range that is $[10^{-3}, 1.2 \times 10^4]$ Hertz (continuous line). The L-curves can be decomposed into three parts: on the left, the fit may be good in the space data but the solution in the parameter space is divergent; on the right, the smoothing is too strong and flattens the solution to zero; the satisfactory solution will be found at the left corner, still in the horizontal part of the curve, as shown. See also Figs 2 and 3 for the inversion of the relaxation time distribution and the corresponding reconstruction of the quadrature (imaginary) resistivity.

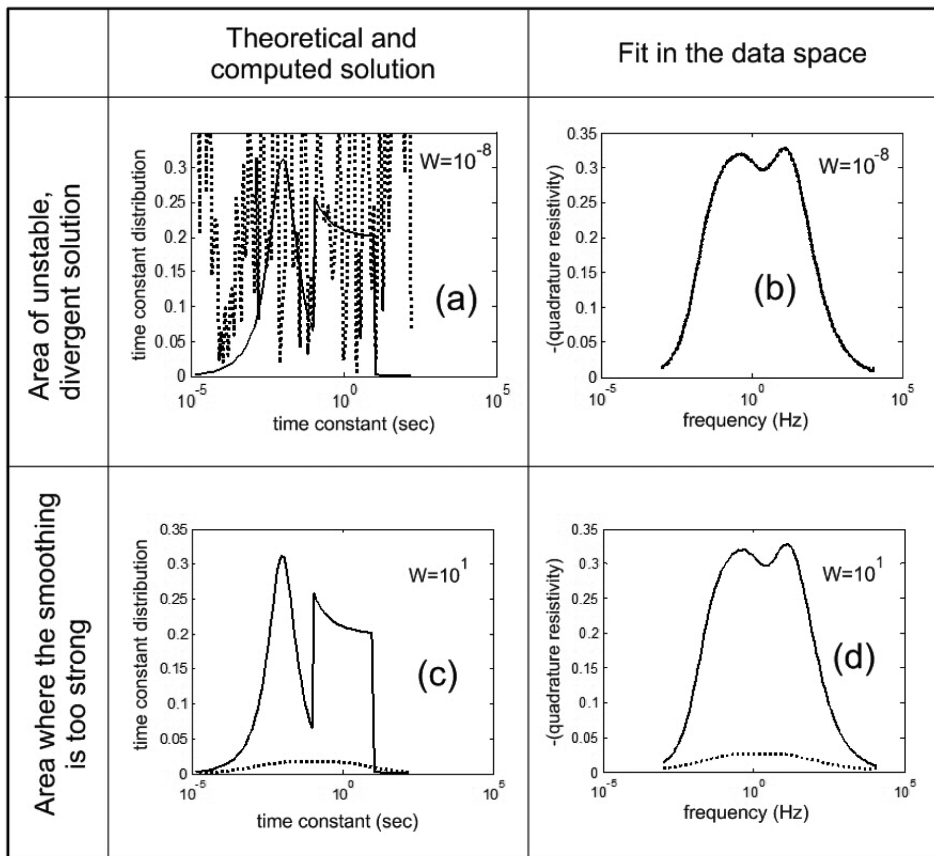


FIGURE 2

The solution in the synthetic (but noisy) case is presented in two unfavourable cases. The model is the one shown in Fig. 1 and involves the sum of a Cole-Cole curve with parameters ($\tau_0=0.1$; $\alpha=0.3 \Leftrightarrow c=0.7$) and a $1/\tau$ model within the interval $\tau \in [0.1; 10]$ s. The model is shown by a continuous line while the inverted solution is in the dotted line. All the spectra are multiplied by τ to facilitate the visualization and only the ‘SIP-FUCHS’ range case is shown. Figures (a) and (b) are relative to the unfavourable case where the value of W is too small with respect to the optimal value. This yields an unstable solution. On the other hand, the cases (c) and (d) are relative to a choice of a value of W chosen that is too high with respect to the optimal value. In this case, the solution is flattened to almost zero.

very broad (and idealistic) range, $[10^{-8}, 10^{+8}]$ Hz and then we also deal with a more restricted range that is the one used by SIP-FUCHS II impedance meter, $[10^{-3}, 1.2 \times 10^4]$ Hz (Cosenza *et al.* 2007; Radic-Research 2008). These two frequency ranges will be denoted as the ‘broad’ and ‘SIP-FUCHS’ ranges, respectively. Figure 1 displays the L-curves showing the classical three distinctive parts: one where the solution diverges, one where the solution is too flattened and the part where the solution is optimal. The L-curve is computed by forming the data misfit term $R(z)$ defined by,

$$R(z) = \left\| Z_z^{n \text{ simulated}}(z) - Z_z^{n \text{ recomputed}}(z) \right\|. \quad (31)$$

The L-curve is precisely the plot of $\left\| Z_z^{n \text{ recomputed}}(z) \right\|^2$ versus the data misfit term $R^2(z)$. The inverted distributions are plotted with the target models. We plotted the L-curve in both wide and narrow (SIP-FUCHS-II) frequency ranges. It is remarkable that the general shape (which is consistent with the expected ‘L-shape’) depends hardly on the operating frequency range. Moreover the best Wiener damping coefficient seems not to depend on the range of frequencies. From the L-curve, the suitable value of the damping parameter is $W = 0.001$ for this synthetic example.

Figure 2 shows what happens if the W damping factor is too small (see cases (a) and (b), with $W = 10^{-8}$) or too strong (see cases (c) and (d), with $W = 10$). The dotted line denotes the

recovered distribution while the continuous line is the target model relative to equation (29). In these cases, the solutions are not satisfactory. Figure 3 shows the case when the damping factor is well chosen. Then the synthetic data and the ‘recomputed’ data match very well and the solution is stable and close to the targeted model. Precisely, the recomputed data are calculated by using the direct calculation, which is, by re-filtering the solution through the low-pass $1/\cosh$ function. This is:

$$Z_z^{n \text{ recomputed}}(z) = -\frac{\pi}{2} FT^{-1} \left[\frac{FT \left[H_s^W(s) \right]}{\cosh(\pi^2 \eta)} \right]. \quad (32)$$

The recomputed data are shown with dotted lines while the continuous curves are relative to the synthetic data. Figure 2 (a,b) emphasizes the fact that a good fit of data can be reached while the inverted solution is quite wrong and this illustrates very well the difficulties encountered in this inverse problem (as many others in geophysics). On the other hand, Fig. 2(c,d) shows the results if W is taken much above the critical value at the corner of the L-curve. In this case, both the target and inverted results are flattened. The information is lost because the denominator in equation (22) becomes too large. The results are oversmoothed (all these results are relative to the SIP-FUCHS frequency range discussed above).

The central flattening of the L-curve (where the result of the inversion is satisfactory) results from the fact that the norm of the solution is not varying while W varies. As explained in Appendix

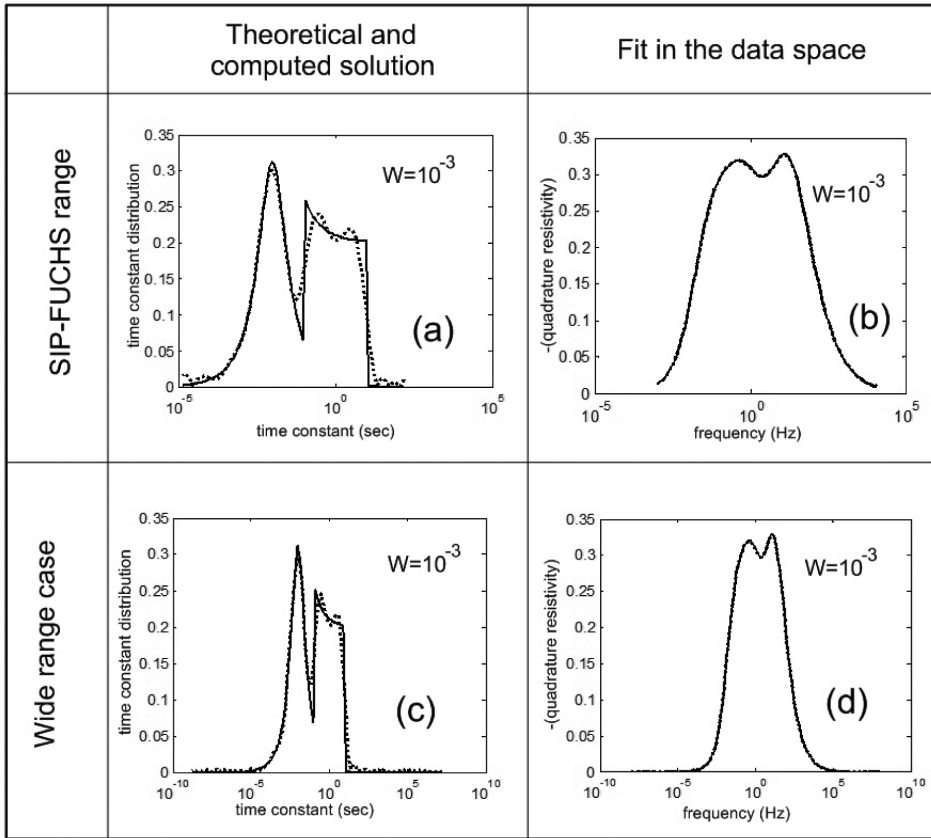


FIGURE 3 The solution in the synthetic (but noisy) case is presented in the favourable case corresponding to the optimal choice of the W -parameter, at the corner of the L-curve (see Fig. 1). The model is shown by a plain line while the inverted solution corresponds to the dotted line. Figures (a) and (b) are relative to the SIP-FUCHS-II frequency range, typically $[10^{-3}, 1.2 \times 10^4]$ Hertz while (c) and (d) correspond to a broader range of frequencies, $[10^{-8}, 10^8]$ Hertz.

C, the left part of the curve is relative to the divergence of the solution: its norm blows up more or less randomly (in other words, it is unstable). The right part of the L-curve would correspond to a solution that is oversmoothed. The solution is flattened and tends to zero, which is why the norm of the residual is constant but not zero, while the norm of the solution tends to zero. This synthetic result also demonstrates that the spectral responses are well-recovered while the distributions of the relaxation times remain slightly noisy.

TEST USING REAL DATA

Tests on experimental data are less straightforward than on synthetic data as explained below. We limit our testing in this paper to laboratory measurements, which do not include electromagnetic coupling effects due to the small size of the quadrupole measurements. However, the data usually exhibit high-frequency behaviour (see Appendices A and B). This high-frequency dielectric effect (Olhoeft 1979; Campbell and Horton 2000) may be approximated by an additive term $i\omega\epsilon_\infty$ to the spectral conductivity (see Appendix A and also Kruschwitz *et al.* 2010). This additive term does not lead to a suitable time constant distribution (see discussion in Appendix B) and should be adjusted and removed from original spectral data prior to attempting to retrieve the distribution of relaxation times $g_\tau(\tau)$.

While the retrieval of the $g_\tau(\tau)$ distribution provided by the resolution of equation (6) and the above described procedure can

be applied on any function, actual application may be performed separately on spectral resistivity or conductivity. Many recent works have connected the spectral conductivity to some textural properties of porous media such as the grain size distribution (e.g., Revil and Florsch 2010) or the pore size distribution (Revil *et al.* in press in Water Resources Research 2011), which should obviously lead to the retrieval of the $g_\tau(\tau)$ distribution based on spectral conductivity for direct comparison. However, following Pelton *et al.* (1978), the polarization phenomena are most of the time explicitly described by the resistivity relaxation phenomena through various models (e.g., Dias 2000; Table 1). Hence, Cole-Cole parameters are more often determined on spectral resistivity and it is usually the so-called resistivity Cole-Cole relaxation time that is for instance directly compared to textural parameters (e.g., Binley *et al.* 2005; Koch *et al.* 2011). Using a Cole-Cole distribution for the relaxation time, the Debye model given by Eq. (5) can be generalized to,

$$\frac{\rho(\omega) - \rho_\infty}{\rho_0 - \rho_\infty} = \frac{1}{1 + (i\omega\tau_c(\rho))^c} = \int_0^\infty \frac{g_\tau^{(\rho)}(\tau)}{1 + i\omega\tau} d\tau, \tag{33}$$

and the associated complex conductivity is then described by a Cole-Cole distribution model:

$$\frac{\sigma(\omega) - \sigma_\infty}{\sigma_0 - \sigma_\infty} = \frac{1}{1 + (i\omega\tau_c(\sigma))^c} = \int_0^\infty \frac{g_\tau^{(\sigma)}(\tau)}{1 + i\omega\tau} d\tau, \tag{34}$$

with the following relation between the two relaxation time constants in the time and frequency domains:

$$\tau_{(\sigma)} = (1 - m)^{1/c} \tau_{(\rho)} \tag{35}$$

with m classically defined as $1 - \rho_{\infty} / \rho_0$. Despite a shift in time, both time constant distributions $g_{\tau}^{(\rho)}$ and $g_{\tau}^{(\sigma)}$ can be superimposed, expressed by Model 2 in Table 1, and the same $g_{\tau}(\tau)$ distribution could be indifferently retrieved from complex resistivity or conductivity data. However, for the more general case, the equivalence does not apply and special care should be taken while choosing to deal with either complex resistivity or conductivity data.

The inversion of experimental data was performed with the optimum Wiener parameter determined through the L-Curve analysis and the reconstructed quadrature spectra agree well with experimental data. Standard Fourier transforms however use a regularly spaced value in the data space. Raw and irregularly spaced experimental data should therefore be interpolated in the logarithmic frequency space before processing. Special care is necessary for the continuation to zero at both sides of the quadrature spectra after removal of the high-frequency effect. This necessary continuation is performed by extrapolation of the data over several decades on both sides of the spectrum in order to control tapering and to prevent a strong Gibbs effect due to the limited ranges of experimental data in the frequency domain.

The first inversion is performed with the data found in Anderson *et al.* (2001). He selected a mine iron waste materials sample, rehydrated with 10% water (Fig. 4a). Resistivity data were fitted by Anderson *et al.* (2001) with the sum of two Cole-Cole models after removal of the dielectric effect as described by Campbell and Horton (2000):

$$\sigma^*(\omega) = \frac{1}{\rho(\omega)} + i\omega\epsilon_{\infty} = \frac{1}{\rho(\omega)} + i\omega K_{\infty}\epsilon_0, \tag{36}$$

(K_{∞} denotes high-frequency permittivity) with the complex resistivity given by,

$$\rho(\omega) = \rho_0 \left[1 - m_1 \left(1 - \frac{1}{1 + (j\omega\tau_1)^{c_1}} \right) - m_2 \left(1 - \frac{1}{1 + (j\omega\tau_2)^{c_2}} \right) \right] \tag{37}$$

The recovered time constant distribution obtained with the resistivity data can be compared with the theoretical distribution for a sum of Cole-Cole models (Fig. 4b) and provides a better fit on experimental data than the double Cole-Cole reference model (Fig. 4c). The L-curve analysis shows a clear L-shape (Fig. 4d) and therefore a clear optimal choice of the damping factor W . Therefore, our actual retrieved distribution appears to be more complex than provided by fitting the double Cole-Cole distribution.

A second inversion is performed on a wetting oil-bearing sand sample (Revil *et al.* 2011), after removal of the high-fre-

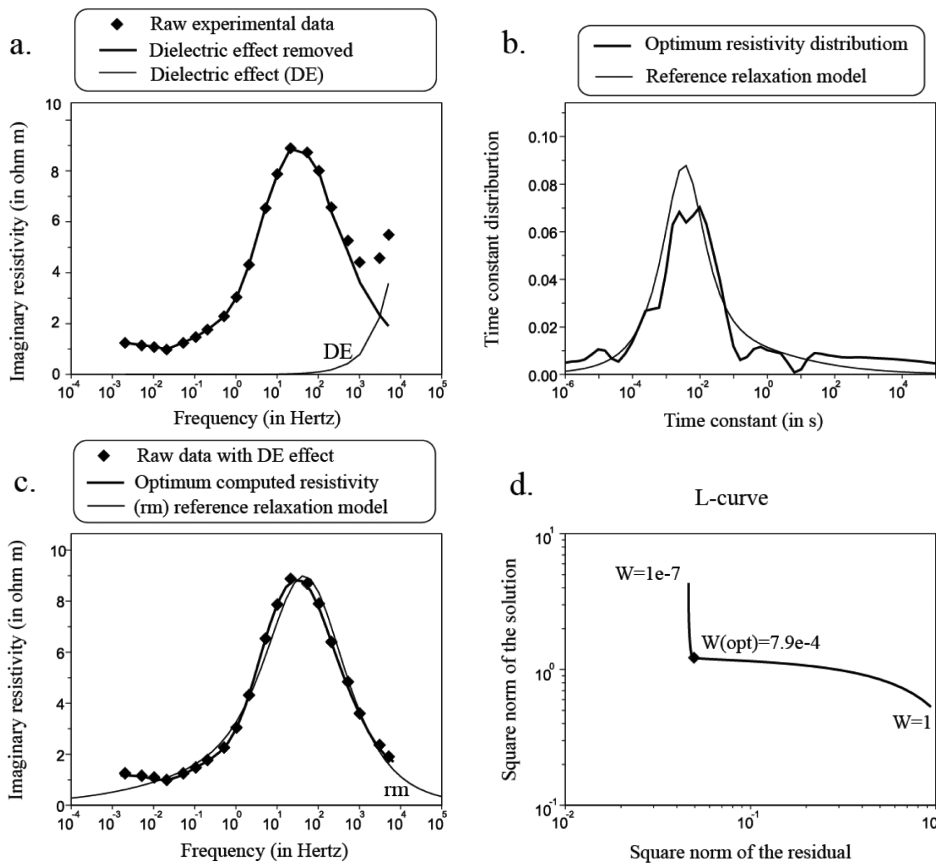


FIGURE 4
Inversion of experimental data from laboratory measurements using a mine iron incline waste sample re-hydrated with 10% water (from Anderson *et al.* 2001). **a.** Experimental raw data, high-frequency dielectric effect and corrected data after dielectric effect removal ($K_{\infty} = 3000$). **b.** Optimum recovered time constant distribution from resistivity data after L-curve analysis. The reference distribution ($m_1 = 0.09$, $\tau_1 = 0.23$ sec, $c_1 = 0.3$, $m_2 = 0.29$, $\tau_2 = 3.3 \times 10^{-3}$ sec., $c_2 = 0.62$) corresponds to the double Cole-Cole distribution provided by Anderson *et al.* (2001). **c.** Processed and reconstructed data from time constant distributions. **d.** L-curve analysis and optimum W -parameter ($W = 7.9 \times 10^{-4}$).

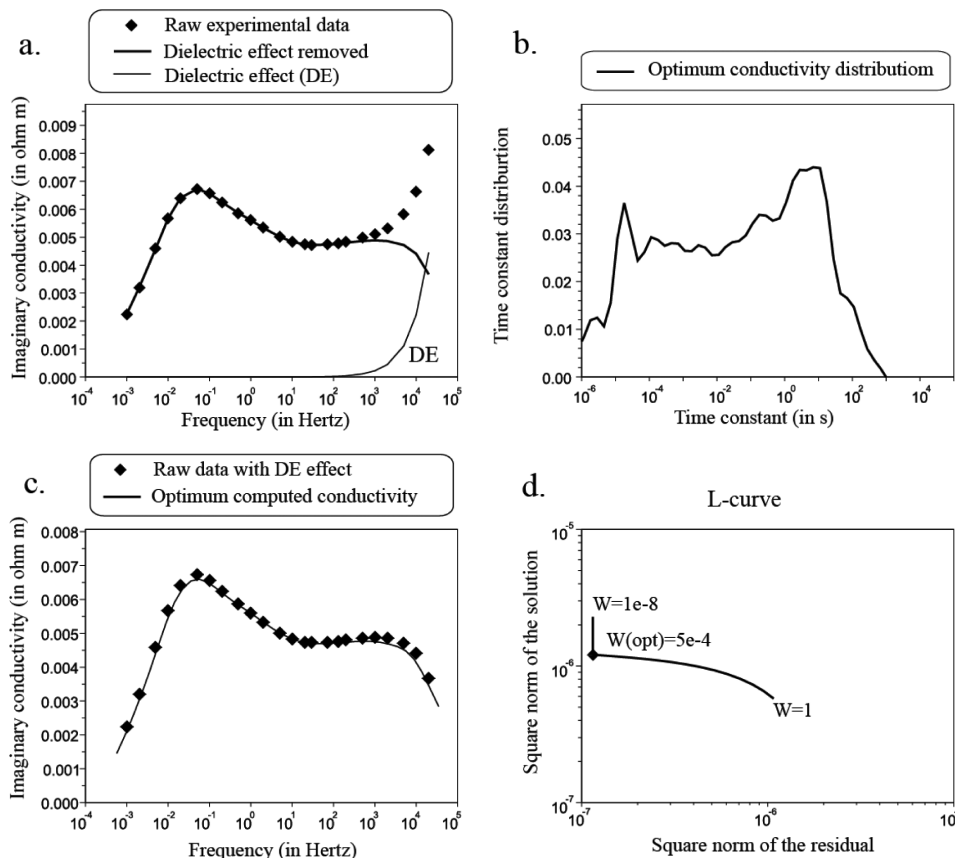


FIGURE 5

Experimental and reconstructed quadrature conductivity spectra for oil-bearing sand (data from Revil *et al.* 2011).

a. Experimental raw data, high-frequency dielectric effect and corrected data after dielectric effect removal ($K_{\infty} = 4$).

b. Optimum recovered time constant distribution from conductivity data after L-curve analysis.

c. Processed and reconstructed data from time constant distributions.

d. L-curve analysis and optimal W -parameter ($W=5 \times 10^{-4}$).

quency dielectric effect. The corrected conductivity spectrum appears quite complicated and attempts to fit a multi Cole-Cole model or a more complicated analytical distribution could be cumbersome. After our Fourier transform processing, the conductivity time constant distribution is distributed between 10^{-6} s and 10^3 s with a peak around 3×10^{-5} s and another peak around 5–12 s (see Fig. 5c). Once again, the L-curve analysis provides a clear choice for the optimal value of the damping factor (Fig. 5d). Because of the effect of oil and grain size, it is difficult to give a physical explanation to the physical nature of these peaks in the distribution of relaxation times. One may be due to the grains and the other one due to the roughness of the grains (see discussion in Leroy *et al.* 2008). In the case for which the distribution of relaxation time can be clearly mapped into a distribution of grain sizes (see Revil and Florsch 2010), we provide in Appendix D the relationships between the conductivity distribution of relaxation times and the distribution of grain sizes. In the case where the relaxation times would be controlled by the pore sizes, similar relationships could be derived to map the distribution of relaxation times into a distribution of pore sizes.

CONCLUSIONS

We have developed a new approach to invert the distribution of relaxation times in induced polarization without the need for an

analytical solution like a Cole-Cole model. The classical least-square inversion scheme is replaced by a fast Wiener deconvolution, which is very important to invert a huge number of spectra in time-lapse spectral induced polarization. This approach is successfully validated on analytical problems, synthetic case studies and real data. When applied to real data, a key step of our approach is to remove the high-frequency dielectric component of the spectra. This approach, which is computationally quite simple to implement, could be coupled to time-lapse 3D frequency domain induced polarization algorithms (e.g., Karaoulis *et al.* 2011) to determine the change on the distribution of relaxation times of the subsurface, for instance for salt tracer plume monitoring, bioremediation and the production of heavy oils. We plan to expand this approach in the future to broadband frequency measurements, including both low-frequency IP and high-frequency dielectric effects. This approach could also be applied.

ACKNOWLEDGEMENTS

We thank John Stockwell at the Colorado School of Mines for fruitful discussions about the log-normal (unsolved) case. A. Revil thanks the Office of Science (BER), U.S. Department of Energy (awards DE-FG02-08ER646559 and DE-FOA-0000311). We thank the Editor Andreas Hördt and two anonymous referees for their very constructive reviews.

APPENDIX A

The high-frequency dielectric effect.

While the equations presented in the main text are general (not dependent on the physics of the polarization process), it is instructive to show how they would apply to a specific polarization model. In the case of water-saturated sands, we can use the model developed recently by Revil and Florsch (2010). To model the entire frequency spectrum investigated experimentally, we need to add to the low-frequency polarization of the electrical double layer of the grains a high-frequency dielectric effect. The complex effective conductivity and the apparent phase lag of the porous material are given by (Revil and Florsch 2010),

$$\sigma^*(\omega) = \sigma_{\text{eff}}(\omega) + i\omega\varepsilon_{\text{eff}}(\omega), \quad (\text{A1})$$

$$\varphi = \text{atan} \left[\frac{\omega\varepsilon_{\text{eff}}}{\sigma_{\text{eff}}} \right]. \quad (\text{A2})$$

The effective conductivity and the effective permittivity are defined by

$$\sigma_{\text{eff}}(\omega) = \text{Re}[\sigma^*(\omega)], \quad (\text{A3})$$

$$\varepsilon_{\text{eff}}(\omega) = \text{Im}[\sigma^*(\omega)/\omega], \quad (\text{A4})$$

In these equations $\text{Re}[\cdot]$ and $\text{Im}[\cdot]$ represent the real and imaginary components of the complex number in the argument. Introducing F as the formation factor, the effective complex conductivity is given by:

$$\sigma^*(\omega) = \frac{1}{F} [\sigma_f^* + (F-1)\sigma_s^*(\omega)]. \quad (\text{A5})$$

The complex conductivity of the solid grain σ_s^* (due to the electrical double layer coating the surface of the grains) and the complex conductivity of the pore water σ_f^* are defined by,

$$\sigma_s^* = \sigma_s' + i(\sigma_s'' + \omega\varepsilon_s), \quad (\text{A6})$$

$$\sigma_f^* = \sigma_f + i\omega\varepsilon_f, \quad (\text{A7})$$

respectively, σ_f denotes the conductivity of the pore water, ε_f denotes the dielectric constant of the pore water and ε_s the dielectric constant of the grains. We can use $\varepsilon_f = 80 \pm 1 \varepsilon_0$ (pure water) and $\varepsilon_s = (4.6 \pm 0.8) \varepsilon_0$ (silica) and $\varepsilon_0 = 8.854 \times 10^{-12} \text{ F m}^{-1}$. The surface conductivity is described by a distribution of relaxation times

$$\sigma_s = \sigma_s' + i\sigma_s'', \quad (\text{A8})$$

$$\sigma_s = b_s + a_s \int_0^\infty \frac{g_\tau(\tau)}{1+i\omega\tau} d\tau, \quad (\text{A9})$$

with $b_s = \sigma_s^\infty$ and $a_s = \sigma_s^0 - \sigma_s^\infty$. Combining equations (A5)–(A9) yields

$$\sigma^*(\omega) = b + a \int_0^\infty \frac{g_\tau(\tau)}{1+i\omega\tau} d\tau + i\omega\varepsilon_\infty, \quad (\text{A10})$$

$$b = \sigma_\infty = \frac{1}{F} [\sigma_f + (F-1)\sigma_s^\infty], \quad (\text{A11})$$

$$a = \frac{F-1}{F} a_s, \quad (\text{A12})$$

$$\varepsilon_\infty = \frac{1}{F} [\varepsilon_f + (F-1)\varepsilon_s]. \quad (\text{A13})$$

The dielectric constant ε_∞ denotes the high-frequency constant of the porous material and $b = \sigma_\infty$ denotes the high-frequency electrical conductivity. Note that the chargeability is given by,

$$m = \frac{\rho_0 - \rho_\infty}{\rho_0} = \frac{\sigma_\infty - \sigma_0}{\sigma_\infty}, \quad (\text{A14})$$

$$m = \frac{(F-1)(\sigma_s^\infty - \sigma_s^0)}{\sigma_f + (F-1)\sigma_s^\infty}, \quad (\text{A15})$$

$$m = -\frac{a}{b}. \quad (\text{A16})$$

APPENDIX B

Retrieval of the time constant distribution accounting for the high-frequency dielectric effect

As shown in equation (A10) of Appendix A, we need to consider an additional frequency-dependent term to the low-frequency polarization for which we are looking for the relaxation time distribution. This term corresponds to the following frequency-dependent impedance,

$$M_\omega(\omega) = iC\omega, \quad (\text{B1})$$

where C is a capacitance. The admittance of a rock sample at low frequency takes therefore the following form, similar to equation (A10) of Appendix A:

$$Y_\omega(\omega) = b + a \int_0^\infty \frac{g_\tau(\tau)}{1+i\omega\tau} d\tau + iC\omega = Y_\omega(\omega) + M_\omega(\omega). \quad (\text{B2})$$

The question we want to tackle in this appendix is the following: starting with equation (B2), can we still find a distribution of relaxation times using the approach developed in the main text? Using the changes of variables provided by equations (10) and (11) of the main text, we can write,

$$Y_z(z) = b + a \int_{-\infty}^\infty \frac{G_s(s)}{1+ie^{-(z-s)}} ds + i\frac{C}{\tau_0} \exp(-z). \quad (\text{B3})$$

As discussed in the main text, we only consider the imaginary parts of equation (B3). To account for the last term of equation (A3), a method could be simply to adjust a value of C in order to fit the high-frequency end of the frequency response (using the very few high-frequency points). In a second step, we would just remove this linear response from the data and then consider the approach developed in the main text for which this term has been omitted.

An alternative and *a priori* possible solution should consist in accounting for this high-frequency term directly into the function for which we look for the distribution of relaxation times. This goal can be reached only if we can find a function $C_\tau(\tau)$ satisfying to:

$$iC\omega = \int_0^\infty \frac{C_\tau(\tau)}{1+i\omega\tau} d\tau. \tag{B4}$$

Can we really find such a function? Taking into account the change of variable given by equation (10) and dealing with the imaginary part only, we obtain:

$$\frac{C}{\tau_0} \exp(-z) = - \int_{-\infty}^{+\infty} \frac{C_s(s)}{2 \cos(z-s)} ds \rightarrow \Psi_z(z). \tag{B5}$$

Using the same approach as in the main text, the solution is formally given by:

$$C_s(s) = -\frac{2}{\pi} FT^{-1} \left[\tilde{\Psi}_\eta(\eta) \cosh(\pi^2 \eta) \right], \tag{B6}$$

where $\tilde{\Psi}_\eta(\eta)$ is the Fourier transform of $\Psi_z(z)$. Clearly, this Fourier transform does not exist. To bypass this difficulty, one can multiply $\Psi_z(z)$ by an appropriate weighting function that renders the Fourier integral convergent. A good weighting function is bell-shaped and dependent on an auxiliary parameter λ . Then, we could delete this term at the end of the calculations. The following function:

$$\varphi_\lambda(z) = e^{-\left(\frac{z}{\lambda}\right)^2} \tag{B7}$$

may be appropriate. To test this possibility, we form the new function:

$$\Phi_{z,\lambda}(z) = \psi_z(z) \varphi_\lambda(z) = \frac{C}{\tau_0} e^{-z} e^{-\left(\frac{z}{\lambda}\right)^2}. \tag{B8}$$

We have:

$$\lim_{\lambda \rightarrow +\infty} \Phi_{z,\lambda}(z) = \Psi_z(z). \tag{B9}$$

The Fourier transform of $\Phi_{\alpha z}(z)$ is given by:

$$\tilde{\Phi}_{\eta,\lambda}(\eta) = \frac{C\lambda\sqrt{\pi}}{\tau_0} \exp \left[-\left(\frac{(\eta-i)\lambda}{2} \right)^2 \right] \tag{B10}$$

Then, the solution that we are looking for (still involving the auxiliary parameter λ) is given by,

$$C_{s,\lambda}(s) = -\frac{2}{\pi} FT^{-1} \left\{ \frac{C\lambda\sqrt{\pi}}{\tau_0} \exp \left[-\left(\frac{(\eta-i)\lambda}{2} \right)^2 \right] \cosh \left(\frac{\pi\eta}{2} \right) \right\}, \tag{B11}$$

$$C_{s,\lambda}(s) = -\frac{2C}{\pi\tau_0} \sin \left[\frac{s\pi}{\lambda^2} \right] \exp \left[\frac{-\lambda^2 s - s^2 + \pi^4 / 4}{\lambda^2} \right]. \tag{B12}$$

Now using $\lambda \rightarrow +\infty$, we obtain,

$$C_{s,\lambda}(s) \xrightarrow{\lambda \rightarrow +\infty} -\frac{2C}{\tau_0} \frac{s}{\lambda^2} e^{-s}. \tag{B13}$$

This function can be expression as a function of the relaxation time τ by,

$$C_{\tau,\lambda}(\tau) = -\frac{2C}{\lambda^2} \frac{1}{\tau} \log \left(\frac{\tau}{\tau_0} \right). \tag{B14}$$

Although the term,

$$C_{s,\lambda}(s) = -\frac{2C}{\pi\tau_0} \sin \left[\frac{s\pi}{\lambda^2} \right] \exp \left[\frac{-\lambda^2 s - s^2 + \pi^4 / 4}{\lambda^2} \right] \tag{B15}$$

can be computed for any value of λ , it is clear that in the limit $\lambda \rightarrow +\infty$ the previous function is not compatible with the frequency trend given by $M_\omega(\omega) = iC\omega$. Therefore, there is no way to eliminate the high-frequency dielectric term by keeping this term in the general formalism used to determine the distribution of the relaxation times. It seems therefore that the only way to proceed is to fit the high-frequency term and to remove it from the data before determining the distribution of the relaxation times. This also implies that high-frequency (at least to 10 kHz) measurements need to be performed to remove this contribution from the data. Methods that do not consider the removal of this high-frequency response provide a biased estimate of the relaxation time distribution.

APPENDIX C

Wiener deconvolution scheme and the use of the L-curve

The Wiener filtering (or deconvolution) is a useful method to perform stable deconvolution. It can be expressed in the time domain (Wiener 1949), or equivalently in the frequency domain. In this later case, we can process directly the frequency domain IP data. We provide here a general view of the problem with more general notations. The deconvolution can be stated as follows,

$$y^{\text{measured}}(t) = \varphi(t) \otimes x(t) + \text{noise}(t) \Leftrightarrow Y^{\text{measured}}(\omega) = \Phi(\omega)X(\omega) + \text{Noise}(\omega), \tag{C1}$$

where $\Phi(t)$ denotes the impulse function of the system and ‘ \otimes ’ denotes the convolution product. The goal is to recover the function $x(t)$ (or $X(\omega)$ in the Fourier domain) from $y^{\text{measured}}(t)$ (or $Y^{\text{measured}}(\omega)$), the latter being the output measured signal through a convolution filter and is additionally affected by the noise(t) (or alternatively in the frequency domain Noise(ω)). In the present case, we process frequency domain IP data and therefore we look for an operator $\Psi(\omega)$ in such a way that we can retrieve the function $X(\omega)$:

$$X(\omega) = \Psi(\omega) \cdot Y^{\text{measured}}(\omega). \tag{C2}$$

If we assume that $\Phi(\omega)$ never vanishes over the studied frequency range, one may use the following trivial choice, which is also the exact solution in the absence of noise:

$$\Psi(\omega) = \frac{1}{\Phi(\omega)}. \quad (\text{C3})$$

That said, in general these conditions are not fulfilled and therefore $\Psi(\omega)$ cannot be derived from such a simple division. Wiener defined his deconvolution filter as,

$$\Psi(\omega) = \frac{\Phi^*(\omega)S(\omega)}{[\Phi^2(\omega)]S(\omega) + N(\omega)}, \quad (\text{C4})$$

where $N(\omega)$ and $S(\omega)$ are the power spectral densities of the signals noise(t) and $x(t)$, respectively and (*) is used to define the complex conjugate of the function. Note that if $S(\omega)$ never vanishes, the preceding equation may be written as:

$$\tilde{Z}_\eta''(\eta) = -\frac{a\pi}{2} \tilde{G}_\eta(\eta) \cdot \frac{1}{\cosh(\pi^2\eta)} \quad (\text{C5})$$

In the case where $N(\omega)$ is small (low noise), we recover equation (C3). It is frequent that no information is available to predict the ratio $N(\omega) / S(\omega)$ and then it can be taken as a constant, saying λ^2 . In such a situation, the Wiener deconvolution is equivalent to the Thikonov regularization and λ^2 identifies itself to the damping factor. This is also why we can apply the L-curve method to our problem.

In our case, in equation (19), we have,

$$\tilde{Z}_\eta''(\eta) = -\frac{a\pi}{2} \tilde{G}_\eta(\eta) \cdot \frac{1}{\cosh(\pi^2\eta)} \quad (\text{C6})$$

and we want to retrieve the function $\tilde{G}_\eta(\eta)$. To do this, we have to divide $\tilde{Z}_\eta''(\eta)$ by:

$$\frac{1}{\cosh(\pi^2\eta)}. \quad (\text{C7})$$

That is, this latter function fulfils the role of $\Phi(\omega)$ in the presentation above. We can therefore write this equivalence as,

$$\Phi(\omega) \equiv \frac{1}{\cosh(\pi^2\eta)}. \quad (\text{C8})$$

Note that in this case $\Phi = \Phi^*$. Then, we apply an operator of the form (dropping the explicit dependence in ω):

$$\Psi = \frac{\Phi^*}{|\Phi^2| + \lambda^2} = \frac{\frac{1}{\Phi}}{1 + \frac{\lambda^2}{\Phi^2}} = \frac{\frac{1}{\Phi}}{1 + W}, \quad (\text{C9})$$

introducing W as our damping factor. Including the appropriate constants, this leads to the operator used in the main text for the IP problem:

$$H_s^W(s) = FT^{-1}[\tilde{H}_\eta^W(\eta)] = FT^{-1}\left[-\frac{2}{\pi} \frac{\tilde{Z}_\eta''(\eta) \cosh(\pi^2\eta)}{1 + \cosh^2(\pi^2\eta)W}\right]. \quad (\text{C10})$$

The reason why the Wiener filter stabilizes the inversion appears clearly when considering this operation. Indeed, without Wiener filtering, the spectrum of the original signal to be deconvoluted has to be divided by '1/cosh'. A multiplication by the function 'cosh', which increases like an exponential of the frequency, is responsible for the following spurious problem. The high-frequency part of the spectrum that contains some noise, which would blow up, is multiplied by the function cosh. Conversely, in equation (C5) (in general) or equation (C10) (this study), the multiplicative function is damped at high frequencies only due to the term including W . Actually, the main difficulty is to choose wisely the damping factor W . If the damping factor is too high, it may squeeze the solution (that is, from the flat right part of the L-curve to the descent on its right side). If the damping factor is too low, it lets the solution blow up. Therefore, the corner point of the L-curve corresponds to the point where the solution is properly damped and the synthetic (re-computed) signal fits well the original data. The shape of the L-curve we obtained for our problem is similar to the shape of the L-curves shown in Fig. 1 of Agarval (2003) or Fig. 1 of Hansen and O'Leary (1993).

APPENDIX D

Relation between the time constant distribution and grain size distribution.

Deciding whether the distribution of relaxation time should be inverted from complex conductivity or from complex resistivity is truly a question of physics. This is why we distinguish the resistivity distribution of relaxation time from the conductivity distribution of relaxation times. In the model developed recently by Revil and Florsch (2010), the relevant physical distribution was the conductivity distribution of relaxation times. We assume that the relationship between grain diameter d and time constant τ is given by:

$$\tau = \tau_0 e^s = \frac{d^2}{8D} \quad (\text{D1})$$

where D denotes the diffusion of the counterions in the electrical double layer. The functions $g_\tau(\tau)$ and $h_d(d)$ denote the distribution of τ and d , respectively. These distributions are both probability density functions and to switch from one parameter to another we must follow a transformation that is valid in terms of probability. We assume that the diffusion coefficient of the counterions in the electrical double layer D is constant. Then the relationship between the two densities is given by:

$$g_\tau(\tau) |\partial\tau| = h_d(d) |\partial d|. \quad (\text{D2})$$

This yields, by taken into account relation (D1) and its derivative, the following two transformations: (i) to go from $g_\tau(\tau)$ to $h_d(d)$ we shall use:

$$h_d(d) = g_\tau\left(\frac{d^2}{8D}\right) \frac{d}{4D} \quad (\text{D3})$$

while (ii) to go from $h_d(d)$ to $g_\tau(\tau)$, we shall use:

$$g_{\tau}(\tau) = h_d \left(\sqrt{8\tau D} \right) \frac{2D}{\sqrt{2\tau D}} \quad (\text{D4})$$

A similar relationship could be written between the probability density of the relaxation time and the probability density of the pore size distribution if the pore size replaces the grain size in equation (D1).

We can follow a similar procedure to establish the relationships between $h_d(d)$ and the distribution $G_s(s)$ given by equation (12). First we write:

It follows the two transformations: (i) the relationship from $G_s(s)$ to $h_d(d)$ is given by ,

$$G_s(s) | \partial s = h_d(d) | \partial d. \quad (\text{D5})$$

while (ii) the relationship between $h_d(d)$ and $G_s(s)$ is given by,

$$h_d(d) = \frac{2}{d} G_s \left[\ln \left(\frac{d^2}{8\tau_0 D} \right) \right] \quad (\text{D6})$$

REFERENCES

- Agarwal V. 2003. Total variation regularization and L-curve method for the selection of regularization parameter. ECE 599. <<http://imaging.utk.edu/people/former/vivek/EdgeTV.pdf>>.
- Anderson A.L., Campbell D.L. and Beanland S. 2001. Laboratory measurements of electrical properties of composite mine dump samples from Colorado and New Mexico. US Geological Survey Open-file Report 01-158, 55p.
- Barsoukov E. and MacDonald J.R. 2005. *Impedance Spectroscopy Theory, Experiment, and Applications, Second Edition*. Edited by John Wiley & Sons, Hoboken, 606 pp.
- Binley A., Slater L.D., Fukes M. and Cassiani G. 2005. Relationship between spectral induced polarization and hydraulic properties of saturated and unsaturated sandstone. *Water Resources Research* **41**, W12417.
- Börner F.D., Schopper W. and Weller A. 1996. Evaluation of transport and storage properties in the soils and groundwater zone from induced polarization measurements. *Geophysical Prospecting* **44**(4), 583–601. Doi:10.1111/j.1365-2478.1996.tb00167.x.
- Campbell D.L. and Horton R.J. 2000. Graphs and tables used to describe electrical measurements of samples of unconsolidated material. US Geological Survey Open-file Report 00-377, 16p.
- Chen J., Kemna A. and Hubbard S.S. 2008. A comparison between Gauss-Newton and Markov-chain Monte Carlo-based methods for inverting spectral induced-polarization data for Cole Cole parameters. *Geophysics* **73**(6), F247–F259.
- Cole K.S. and Cole R.H. 1941. Dispersion and absorption in dielectrics. I. Alternating current characteristics. *Journal of Chemical Physics* **9**, 341–351.
- Cosenza Ph., Ghorbani A., Florsch N. and Revil A. 2007. Effects of drying on the low-frequency electrical properties of Tournemire argillites. *Pure and Applied Geophysics* **164**, 2043–2066.
- Cosenza P., Ghorbani A., Revil A., Zamora M., Schmutz M., Jougnot D. and Florsch N. 2008. A physical model of the low-frequency electrical polarization of clay rocks. *Journal of Geophysical Research* **113**, B08204. Doi:10.1029/2007JB005539.
- Davidson D.W. and Cole R.H. 1950. Dielectric relaxation in glycerine. *Journal of Chemical Physics* **18**, 1417.
- Debye P. and Falkenhagen H. 1928. Dispersion of the Conductivity and Dielectric Constants of Strong Electrolytes. *Phys. Z.* **29**, 121–132, 401–426.
- Dias C.A. 2000. Developments in a model to describe low-frequency electrical polarization of rocks. *Geophysics* **65**(2), 437–451.
- Dukhin S.S. and Shilov V.N. 2002. Nonequilibrium electric surface phenomena and extended electrokinetic characterization of particles In: *Interfacial Electrokinetics and Electrophoresis* (ed.A.V. Delgado), pp. 991. *Surfactant Science Series* **106**, 55–85.
- Fixman M. 1980. Charged macromolecules in external fields. I: The sphere. *Journal of Chemical Physics* **72**, 5177–5186.
- Fuoss R.M. and Kirkwood J.G. 1941. Dipole moments in Polyvinyl Chloride-Diphenyl systems. In: *Electrical properties of solids. VIII. Journal of the American Chemical Society* **63**, 385–394.
- Ghorbani A., Camerlynck C., Florsch N., Cosenza P., Tabbagh A. and Revil A. 2007. Bayesian inference of the Cole-Cole parameters from time and frequency domain induced polarization. *Geophysical Prospecting*, **55**(4), 589–605. Doi: 10.1111/j.1365-2478.2007.00627.x.
- Ghorbani A., Cosenza P., Revil A., Zamora M., Schmutz M., Florsch N. and Jougnot D. 2009. Non-invasive monitoring of water content and textural changes in clay-rocks using spectral induced polarization: A laboratory investigation. *Applied Clay Science* **43**, 493–502.
- Grisseman C. 1971. Examination of the frequency-dependent conductivity of ore-containing rock on artificial model, Scientific Rep. no. 2. Electronics laboratory University of Innsbruck, Austria. Hallof, P.G., 1965.
- Hansen P.C. and O’Leary, D.P. 1993. The use of the L-curve in the regularization of discrete ill-posed problems. *SIAM Journal on Scientific Computing* **14**, 1487–1503.
- Hördt A., Blaschek R., Kemna A. and Zisser N. 2007. Hydraulic conductivity estimation from induced polarisation data at the field scale. The Krauthausen case history. *Journal of Applied Geophysics* **62**, 33–46.
- Jonscher A.K. 1983. *Dielectric Relaxation in Solids*. Chelsea Press, 219–226.
- Jonscher A.K. 1999. Dielectric relaxation in solids. *Journal of Physics D: Applied Physics* **32**, 57–70. Doi: 10.1088/0022-3727/32/14/201.
- Karaoulis M., Revil A., Werkema D.D., Minsley B., Woodruff W.F. and Kemna A. 2011. Time-lapse 3D inversion of complex conductivity data using an active time constrained (ATC) approach. *Geophysical Journal International* **187**, 237–251.
- Kemna A. 2000. *Tomographic Inversion of Complex Resistivity*. Dissertation, Ruhr Universität Bochum, Germany.
- Koch K., Kemna A., Irving J. and Holliger K. 2011. Impact of changes in grain size and pore space on the hydraulic conductivity and spectral induced polarization response of sand. *Hydrology and Earth System Sciences* **15**, 1785–1794.
- Kruschwitz S., Binley A., Lesmes, L. and Elshenawy A. 2010. Textural controls on low-frequency electrical spectra of porous media. *Geophysics* **75**, WA113–WA123.
- Leroy P., Revil A., Kemna A., Cosenza P. and Ghorbani A. 2008. Spectral induced polarization of water-saturated packs of glass beads. *Journal of Colloid and Interface Science* **321**, 103–117.
- Lesmes D.P. and Morgan F.D. 2001. Dielectric spectroscopy of sedimentary rocks. *Journal of Geophysical Research* **106**(B7), 13329–13346.
- Macdonald J.R. and Brachman M.K. 1956. Linear System Integral Transform Relations. *Review of Modern Physics* **28**, 393–422.
- Marshall D.J. and Madden T.R. 1959. Induced polarization, a study of its causes. *Geophysics* **24**, 790–816.
- Matsumoto A. and Higasi K. 1962. Dielectric relaxation of non-rigid molecules at lower temperature. *Journal of Chemical Physics* **36**, 1776–1780.

- Miranda D.A. and Lopez-Rivera S.A. 2008. Determination of Cole–Cole parameters using only the real part of electrical impedivity measurements. *Physiological Measurement* **29**, 669–683. Doi:10.1088/0967-3334/29/5/011.
- Nordsiek S. and Weller A. 2008. A new approach to fitting induced-polarization spectra. *Geophysics* **73**(6), F235–F245.
- Olhoeft G.R. 1979. Electrical Properties. In: *Initial Report of the Petrophysics Laboratory: U.S. Geological Survey Circular 789*, (Eds. G.R. Hunt, G.R. Johnson, G.R. Olhoeft, D.E. Watson and K. Watson), pp. 1–26.
- Olhoeft G.R. 1985. Low-frequency electrical properties. *Geophysics* **50**, 2492–2503.
- Pelton W.H., Sill W.R. and Smith B.D. 1983. Interpretation of complex resistivity and dielectric data – Part I. *Geophysical Transactions* **29**, 297–330.
- Pelton W.H., Ward S.H., Hallof P.G., Sill W.R. and Nelson P.H. 1978. Mineral discrimination and removal of inductive coupling with multi-frequency IP. *Geophysics* **43**, 588–609.
- Polyanin A.D. and Manzhairov A.V. 1998. *Handbook of Integral Equations*. CRC Press, Boca Raton. ISBN 0-8493-2876-4.
- Proakis J.G. and Manolakis D.G. 2007. *Digital Signal Processing: Principles, Algorithms, and Applications*. Prentice-Hall, 4th Ed.
- Radic-Research. 2008. http://www.radic-research.homepage.t-online.de/Flyer_SIP-Fuchs_III_200810.pdf.
- Revil A. and Florsch N. 2010. Determination of permeability from spectral induced polarization data in granular media. *Geophysical Journal International* **181**, 1480–1498. Doi: 10.1111/j.1365-246X.2010.04573.x.
- Revil A., Leroy P., Ghorbani A., Florsch N. and Niemeijer A.R. 2006. Compaction of quartz sands by pressure solution using a Cole-Cole distribution of relaxation times. *Journal of Geophysical Research* **111**, B09205. Doi:10.1029/2005JB004151.
- Revil A., Schmutz M. and Batzle M.L. 2011. Influence of oil wettability upon spectral induced polarization of oil-bearing sands. *Geophysics* **76**(5), A31–A36.
- Schwarz G. 1962. A theory of the low-frequency dielectric dispersion of colloidal particles in electrolyte solution. *Journal of Physical Chemistry* **66**, 2636–2642.
- Scott J. and Barker R. 2003. Determining pore-throat size in Permian-Triassic sandstones from low-frequency electrical spectroscopy. *Geophysical Research Letters* **30**, 1450. Doi:10.1029/2003GL016951.
- Strauss U.P. 1954. *The Collected Papers of Peter J.W. Debye*. Interscience, New York-London, 700 pp.
- Tabbagh A., Cosenza P., Ghorbani A., Guérin R. and Florsch N. 2009. Modelling of Maxwell–Wagner induced polarisation amplitude for clayey materials. *Journal of Applied Geophysics* **67**, 109–113.
- Tarasov A. and Titov K. 2007. Relaxation time distribution from time domain induced polarization measurements. *Geophysical Journal International* **170**, 31–43.
- Tong M., Li L., Wang W. and Jiang Y. 2006a. A time-domain induced-polarization method for estimating permeability in a shaly sand reservoir. *Geophysical Prospecting* **54**, 623–631.
- Tong M., Li L., Wang W. and Jiang Y. 2006b. Determining capillary-pressure curve, pore-size distribution, and permeability from induced polarization of shaly sand. *Geophysics* **71**, 33–40.
- Urtenov M.A.-Kh., Kirillova E.V., Seidova N.M. and Nikonenko V.V. 2007. Decoupling of the Nernst-Planck and Poisson equations. application to a membrane system at overlimiting currents. *Journal of Physical Chemistry B* **111**, 14208–14222.
- Vanhala H. 1997. *Laboratory and Field Studies of Environmental and Exploration Applications of the Spectral Induced Polarization (SIP) Method*. Ph.D. Dissertation, Helsinki University of Technology.
- Vaudelet P., Revil A., Schmutz M., Franceschi M. and Bégassat P. 2011. Induced polarization signature of the presence of copper in saturated sands. *Water Resources Research* **47**, W02526. Doi:10.1029/2010WR009310.
- Vinegar H.J. and Waxman M.H. 1984. Induced polarization of shaly sands. *Geophysics* **49**, 1267–1287.
- Wiener N. 1949. *Extrapolation, Interpolation, and Smoothing of Stationary Time Series*. New York, Wiley. ISBN 0-262-73005-7.
- Williams G. and Watts D.C. 1970. Non-Symmetrical Dielectric Relaxation Behavior Arising from a Simple Empirical Decay Function. *Transactions of the Faraday Society* **66**, 80–85.
- Yeung Y.Y. and Shin F.G. 1991. Pulse response function of dielectric susceptibility. *Journal of Material Sciences* **26**, 1781–1787.
- Zhdanov M. 2008. Generalized effective-medium theory of induced polarization. *Geophysics* **73**(5), F197–F211.
- Zisser N., Kemna A. and Nover G. 2010. Relationship between low-frequency electrical properties and hydraulic permeability of low-permeable sandstones. *Geophysics* **75**(3), E131–E141.

